Insights into the fate of antimony (Sb) in contaminated soils: ageing influence on Sb mobility, bioavailability, bioaccessibility and speciation

Insights into the fate of antimony (Sb) in contaminated soils: ageing influence on Sb mobility, bioavailability, bioaccessibility and speciation

Stefania Diquattro[a], Paola Castaldi[a], Susie Ritch[b], Albert L. Juhasz[b], Gianluca Brunetti[b], Kirk G. Scheckel[c], Giovanni Garau[a*], Enzo Lombi[b]

[a] Dipartimento di Agraria, University of Sassari, Viale Italia 39/B, 07100, Sassari, Italy

[b] Future Industries Institute, University of South Australia, Mawson Lakes Campus, Adelaide, SA, 5095, Australia

[c] U. S. Environmental Protection Agency, Office of Research and Development, Center for Environmental Solutions and Emergency Response, Cincinnati, OH 45268, United States

[*] Corresponding author: G. Garau (ggarau@uniss.it)

Abstract

The effect of long-term ageing (up to 700 days) on the mobility, potential bioavailability and bioaccessibility of antimony (Sb) was investigated in two soils (S1: pH 8.2; S2: pH 4.9) spiked with two Sb concentrations (100 and 1000 mg·kg^{-1}).

The Sb mobility decreased with ageing as highlighted by sequential extraction, while its residual fraction significantly increased. The concentration of Sb (C_{DGT}), as determined by diffusive gradients in thin films (DGT), showed a reduction in potential contaminant bioavailability during ageing. The DGT analysis also showed that Sb-C_{DGT} after 700 days ageing was significantly higher in S1-1000 compared to S2-1000, suggesting soil pH plays a key role in Sb potential bioavailability. In-vitro tests also revealed that Sb bioaccessibility decreased over time. Linear combination fitting of Sb K-edge XANES derivative spectra showed, as a general trend, an increase in Sb(V) sorption to inorganic oxides with ageing as well as Sb(V) bound to organic matter (e.g. up to 27 and 37 % respectively for S2-100). The results indicated that ageing can alleviate Sb ecotoxicity in soil and that the effectiveness of such processes can be increased at acidic pH. However, substantial risks due to Sb mobility, potential bioavailability and bioaccessibility remained in contaminated soils even after 700 days ageing.

Keywords: Ageing; Antimony; Potential bioavailability; Bioaccessibility; X-ray absorption near-edge structure (XANES) spectroscopy

1. Introduction

Antimony (Sb) is a potentially toxic element (PTE), considered as a priority pollutant by the United States Environmental Protection Agency and the European Union (CEC, 1998; USEPA, 2009). Antimony concentration in the environment is related to both natural phenomena such as weathering, biological activity, or volcanic

activity and anthropogenic inputs (He et al., 2019). In recent years, Sb concentrations in the environment have considerably increased as a result of mining and smelting operations, waste incinerators, coal and petroleum combustion, spent ammunition, polyethylene terephthalate industries, battery factories, and use of pharmaceuticals and pesticides (e.g. Okkenhaug et al., 2016). In this context, knowledge of Sb mobility, potential bioavailability and bioaccessibility in soil is of primary importance for the assessment of ecological risk and potential human health impacts (Diquattro et al., 2020; Fu et al., 2016; Hammel et al., 2000).

Antimony mobility, bioavailability and bioaccessibility in soil depend on its speciation as well as on the pH, redox conditions, amount and type of colloids present and microbial populations (Luo et al., 2014; Wilson et al., 2010). Antimony commonly occurs in the environment as trivalent Sb(III) or pentavalent Sb(V) inorganic species, with antimonite [$Sb(OH)_3$] and antimonate [$Sb(OH)_6^-$] the most common Sb(III) and Sb(V) compounds, respectively (Kang et al., 2000). Antimonate is the predominant form present under aerobic and mildly reducing conditions (Filella et al., 2002; Filella et al., 2009; Telford et al., 2008) and its mobility in soil, in the 5.0-8.5 pH range, is generally greater than that of antimonite due to the negative charge of the former species [pKa $HSb(OH)_6$ = 2.55; pKa $Sb(OH)_3$ = 11.8] (Herath et al., 2017; Johnston et al., 2020).

Binding to soil colloid surfaces (e.g., organic matter, Fe, Al, and Mn oxy-hydroxides) by specific and nonspecific adsorption reactions, as well as structural incorporation into Fe(III)-oxyhydroxide minerals, can have substantial influence on Sb mobility and bioavailability, eventually leading to contaminant attenuation (Wilson et al., 2010). For instance, it was shown that different humic substance

functional groups (e.g., -SH and -COOH groups) can interact with Sb(III) (Tella and Pokrovski, 2009). In regards to Sb(V), specific adsorption by humic acids under acid conditions can occur via the establishment of pentagonal or hexagonal rings involving Sb–O–C linkages (Sh et al., 2012; Steely et al., 2007; Tella and Pokrovski, 2012). Moreover, cationic metals within humic acids [e.g, Fe(III), Mg(II), and Ca(II)], can act as bridging elements between the negatively charged humic molecules and the antimonate complex (Diquattro et al., 2018). Finally, stable interactions (e.g., inner sphere complexes) between Sb(V) and Fe and Al oxy-hydroxides have previously been reported (Bagherifam et al., 2014; Essington and Stewart, 2016; 2018), as well as structural Sb(V) incorporation into Fe(III)-oxide (e.g. goethite) via heterovalent Sb(V)/Fe(III) substitution (e.g. Burton et al., 2020). Overall, the stability of complexes between Sb(V) and soil colloids decreases as the pH raises, due to the increase of electrostatic repulsion phenomena occurring between the $Sb(OH)_6^-$ oxyanion and the negatively charged surface groups of Fe and Al oxy-hydroxides and organic matter (Xi et al., 2016). Moreover, the strength of Sb binding to soil colloid surfaces is fundamental in regulating contaminant bioaccessibility which is an important parameter for the prediction of exposure and health risks from incidental ingestion of Sb contaminated soils (Ruby et al., 1996). In particular, bioaccessibility refers to the fraction of a contaminant that is soluble in the digestive phase and as such potentially available for intestinal absorption (Mele et al., 2015).

Given that the stability of interactions between Sb and soil colloids, and therefore contaminant mobility, bioavailability and bioaccessibility, can change over time, this should be considered in order to gain a greater understanding of ecotoxicological

97 effects of antimony in soil systems and (more in general) in the environment
98 (Violante et al., 2010). The reduction of PTEs mobility, potential bioavailability and
99 bioaccessibility through specific immobilization mechanisms, which occur as a
100 function of their contact time with soil colloids, is called “ageing” (e.g. Peng et al.,
101 2019; Tang et al., 2006). Several PTEs-fixation reactions such as complexation,
102 surface adsorption, precipitation or diffusion and occlusion into meso and
103 micropores, can occur in soil with time (Jalali and Khanlari, 2008). For instance, lead
104 (Pb), zinc (Zn), cadmium (Cd) and copper (Cu) tend to become non-exchangeable
105 with an increase in residence time, due to the transformation of weak interactions
106 (e.g. outer sphere complexes) into more stable ones (e.g. inner sphere complexes)
107 (Jalali and Khanlari, 2008; Tang et al., 2006). Similarly, a decrease in water-soluble
108 and exchangeable arsenic (As) and selenium (Se), and an increase in PTEs bound to
109 amorphous Fe/Al oxy-hydroxides, or in residual fractions, have been observed
110 during ageing (e.g. Peng et al., 2019; Tang et al., 2007).

111 Despite numerous studies over the last decade investigating the effects of ageing
112 on the mobility and bioavailability of many PTEs (e.g. Diagboya et al., 2015;
113 Martínez and McBride, 1998; Yang et al., 2003), limited knowledge is available for
114 Sb. For instance, Sanderson et al. (2014) studied the bioavailability of Pb, Sb, Zn,
115 nickel (Ni), Cu and As in soil after one year ageing, but the study mainly focused on
116 selected ecotoxicological endpoints, i.e. earthworms, plants and microbial activity.
117 Likewise, Zhang et al. (2020) explored Sb toxicity on barley root elongation after 3-
118 months ageing, while Egodawatta et al. (2018) reported higher Sb bioavailability for
119 water spinach when exposed to recently contaminated soil (14 days) compared to
120 historically contaminated (34 years).

In this study we therefore sought to clarify the influence of ageing on the fate and behaviour of Sb in soil by using a combination of well-established and innovative approaches. More specifically, the objective of this work was to investigate the effect of ageing (from 1 day up to 700 days) on the mobility, potential bioavailability, bioaccessibility and speciation of Sb added [as Sb(V)] at two different concentrations (100 and 1000 $mg \cdot kg^{-1}$) on two distinct soils. In particular, the fate of Sb in soil was studied by sequential extraction to identify labile and relatively immobile Sb pools (Diquattro et al. 2020; Garau et al., 2017; Wenzel et al., 2001). Antimony potential bioavailability was addressed with diffusive gradients in thin-films (DGT) probes (Luo et al., 2010), while Sb bioaccessibility was studied by using simulated gastric and intestinal solutions in *in-vitro* tests (Ruby et al., 1996). Finally, synchrotron based X-ray absorption near-edge structure (XANES) spectroscopy was used to define Sb speciation in soil (Maher et al., 2018; Wang et al., 2017). The experimental design and the combined use of the above-mentioned techniques were expected to provide a deeper understanding of environmental risk posed by Sb and of possible attenuation mechanisms governed by time.

2. Materials and methods

2.1. Soil physical-chemical analysis and microcosm set up

Different topsoil samples (0-20 cm depth) were collected randomly from two uncultivated fields located in north-western Sardinia (Sassari), soil 1 (S1): 40°43′32.77″N 8°24′48.6″E; soil 2 (S2): 40°56'15.7"N 8°53'30.4"E. These soils were

selected because they were not previously used for agricultural or anthropogenic activities, they were distant from possible contamination sources (i.e. to reduce the possibility of external Sb input), and they exhibited different physico-chemical properties (Table S1). Soil samples were pooled in the laboratory according to their origin (i.e., S1 and S2), sieved to < 2 mm and analysed as previously reported (Diquattro et al., 2020). Briefly, the S1 soil (sandy clay loam) was alkaline (pH 8.2), while S2 (loamy coarse sand) was acidic (pH 4.9). S1 had a higher cation exchange capacity (CEC) compared to S2, i.e. 20 vs 13 $cmol_{(+)} \cdot kg^{-1}$ soil respectively, while the opposite was found for soil organic matter (SOM), i.e. 1.75 vs 2.19 % and dissolved organic carbon (DOC), i.e. 0.17 vs 0.39 $mg \cdot g^{-1}$ soil respectively. The point of zero charge (pH_{PZC}) was 5.7 for S1 and 2.6 for S2. High concentrations of total Fe (16,350 and 5,650 $mg \cdot kg^{-1}$ respectively) and Al (19,930 and 3,924 $mg \cdot kg^{-1}$ respectively) were recorded in S1 and S2, while total Ca was more abundant in S1 (62,500 $mg \cdot kg^{-1}$) compared to S2 (2,426 $mg \cdot kg^{-1}$). Antimony in S1 and S2 was quantified by Inductively Coupled Plasma Mass Spectrometry (ICP-QQQ-MS) (Agilent 8800) after digestion of soil with aqua regia reverse solution (HNO_3/HCl 3:1 ratio) and microwave mineralisation (MARS-6, CEM) using USEPA method 3051A. A standard reference material (NIST-SRM 2711A) was included for quality assurance and quality control. In both soils, Sb was not detected (< 0.01 $\mu g \cdot kg^{-1}$). Further details on the chemical features of both soils can be found in Diquattro et al. (2020).

Thirty microcosms (each consisting of 300 g soil) were prepared for each soil type (S1 and S2) in plastic pots (10 cm diameter x 10 cm height). All soils were brought to 60 % of their water holding capacity (WHC) with deionised water (Jury et al., 1991). For each soil type, 15 microcosms were spiked with 100 $mg \cdot kg^{-1}$ Sb(V) (S-

100), and another 15 with 1000 $mg \cdot kg^{-1}$ Sb(V) (S-1000). Sb(V) derived from $K[Sb(OH)_6]$ (CAS 12208-13-8; Sigma Aldrich, Saint–Louis, USA) was added as a water solution ($K[Sb(OH)_6]$ solubility in water is 20 g L^{-1}). Antimony concentrations added were selected to mimic a medium-low and a high contamination level based on previous studies (Courtin-Nomade et al., 2012; Diquattro et al., 2020; Garau et al., 2017). Before addition to soil, each Sb(V) solution was adjusted to the same pH of the soil using 0.1 M NaOH or HCl solutions. Microcosms were carefully mixed and then left to age at constant temperature (25 °C) and humidity (60 % WHC; by weight adjustment) for different times: 1, 7, 31, 91 and 700 days (d). The selected time-points were chosen to evaluate both the short and medium to long-term influence of ageing on Sb mobility, bioavailability, bioaccessibility and speciation. At each time-point, triplicate S1 and S2 microcosms (i.e., S1-100, S1-1000, S2-100 and S2-1000) were analysed as follows. Total concentration of Sb was quantified in spiked microcosms (< 2 mm and < 250 µm particle size fractions) at different time-points (Table 1), by ICP-QQQ-MS as previously described. A standard reference material (NIST-SRM 2711A) was included for quality assurance and quality control.

2.2. Sequential extraction of soil Sb

At each time-point, Sb mobility in the different soils was evaluated through the sequential extraction procedure (SEP) proposed by Wenzel et al. (2001) with minor modifications. This method was originally developed for arsenic but has also been widely used for antimony (e.g. Diquattro et al., 2018; Garau et al., 2017; Ngo et al., 2020) because of the similar chemical characteristics of these PTEs (Wilson et al.,

193 2010). Different soil samples (n=10; 1 g each) were randomly collected from each
194 microcosm and pooled together. Then a representative soil sample (1 g) was
195 collected for Sb sequential extraction. The procedure was repeated 3 times for each
196 microcosm. Triplicate soil samples (1 g) collected from each microcosm at different
197 ageing times (i.e., 1, 7, 31, 91, 700 d) were treated with 25 mL of deionised water
198 and shaken for 2 h at 25 °C to extract water-soluble Sb (Fraction 1, F1). Then, the
199 same soil samples were treated with 25 mL of a 0.05 M $(NH_4)_2SO_4$ solution and
200 shaken for 4 h at 25 °C to extract non-specifically sorbed Sb (Fraction 2, F2).
201 Finally, the same soil samples were treated with 25 mL of a 0.05 M $NH_4H_2PO_4$
202 solution and shaken for 16 h at 25 °C h to extract specifically sorbed Sb (Fraction 3,
203 F3). Then, soil samples were digested with reverse aqua regia (HNO_3/HCl 3:1 ratio)
204 and microwave mineralisation (MARS-6, CEM) using USEPA method 3051A, to
205 quantify residual Sb (Fraction 4, F4). After each extraction step, soil suspensions
206 were centrifuged at 1800 *g* for 10 min. Supernatants were then filtered through a 0.45
207 µm filter and Sb concentrations determined in the liquid phase by ICP-QQQ-MS as
208 previously described. A standard reference material (NIST-SRM 2711A) was
209 included for quality assurance and quality control.
210
211 *2.3. DGT measurements*
212
213 At each time-point, Sb potential bioavailability was assessed in different soils
214 through the DGT® technique. This is based on a device (deployed on the soil surface)
215 that accumulates labile soil Sb on a binding gel after its diffusion through a hydrogel,
216 which acts as a diffusion layer (Li et al., 2018). In this study, a titanium oxide

(Metsorb) binding gel (DGT Research Ltd, Lancaster, UK) was employed. The exposure area of the binding gel was 3.14 cm^2 and its thickness was 0.4 mm. Triplicate soil samples (50 g) collected from each microcosm at different ageing times (i.e., 1, 7, 31, 91,700 d) were brought to 100 % of their WHC, then a DGT device was deployed on the soil surface and gentle pressed (to favour the contact between soil and device). DGT probes were left in contact with soils for 24 h at 25 °C. Afterwards, binding gels (of each DGT device) were collected and eluted for 24 h in 2 mL of a 1 M NaOH and 1 M H_2O_2 solution. Eluent solutions were then 10-fold diluted in 2 % ultrapure HNO_3 prior to the analysis of Sb content by ICP-QQQ-MS as previously described.

The time-averaged Sb concentration present in the soil solution at the surface of the DGT device (C_{DGT}, expressed as $\mu g \cdot L^{-1}$; i.e. a measure of labile or bioavailable soil Sb) was obtained according to the following equation (Eq. 1):

$C_{DGT} = M\Delta g/AtD$ (Eq. 1) (Davison and Zhang, 1994)

where M is the mass (µg) of element accumulated on the binding gel, Δg is the thickness of the diffusive gel (0.8 mm) plus the thickness of filter membrane (0.1 mm), D is the element diffusion coefficient in the diffusive layer (5.46×10^{-6} cm^2 s^{-1} for Sb; Luo et al., 2010), A is the exposed area of the binding gel (3.14 cm^2), and t is the deployment time (s). Moreover, the R value, which reflects the ability of soil to resupply antimony to the device interface, was calculated as the ratio between Sb-DGT (C_{DGT}) to Sb concentration in soil pore water (Csol) (Harper et al. 2000).

2.4. In vitro bioaccessibility of soil Sb

241 At each time-point, Sb bioaccessibility in spiked soils was determined using the
242 Solubility Bio-accessibility Research Consortium in vitro assay (SBRC) which
243 includes a gastric (SBRC-G) and an intestinal phase (SBRC-I) (Mele et al., 2015).
244 The < 250 μm (Table 1) soil particle size fraction was employed for analysis, since it
245 represents the fraction that adheres to fingers and is available for incidental ingestion
246 (Mele et al., 2015). Triplicate soil samples (0.4 g) collected (as described for SEP)
247 from microcosms at different ageing times (i.e., 1, 7, 31, 91, 700 d) were treated with
248 40 mL of a gastric solution (30.03 $g \cdot L^{-1}$ glycine adjusted to pH 1.5 with 37 % HCl)
249 and incubated in agitation (40 rpm on a Ratek rotary suspension mixer) at 37 °C and
250 constant pH (i.e., 1.5). After 1-hour incubation, 4 mL of supernatant was collected,
251 filtered through 0.45 μm filters and stored at 4 °C (SBRC-G phase). The remaining
252 suspension was adjusted to pH 7.0 with a 50 % NaOH solution, and intestinal
253 solution (3 mL) containing 70 mg of bile bovine (Sigma-Aldrich) and 20 mg of
254 pancreatin (Sigma-Aldrich) was added. The intestinal phase was then incubated at
255 constant pH (i.e., 7.0) as previously mentioned. After 4 h, supernatant aliquots (10
256 mL) were collected, filtered through 0.45 μm filters and stored at 4 °C (SBRC-I
257 phase). Soluble Sb in SBRC-G and SBRC-I phases was determined by ICP-QQQ-
258 MS (Agilent 8800), while total Sb concentration in soil was quantified after
259 mineralization (< 250 μm) as previously described. A standard reference material
260 (SRM 2711A) was also included for quality assurance and quality control.
261 In vitro Sb bioaccessibility values (%) were calculated by dividing the Sb
262 concentration determined in SBRC-G or SBRC-I phases by the total Sb
263 concentration in the soil (< 250 μm) as in the following equation (Eq. 2):

BA_{Sb} (%) = [soluble Sb in SBRC-G or SBRC-I ($mg \cdot kg^{-1}$)/ total Sb concentration $_{<250\ \mu m}$ ($mg \cdot kg^{-1}$)] x 100 (Eq. 2).

2.5. X-ray absorption spectroscopy

Antimony K-edge X-ray absorption near-edge structure (XANES) spectra were obtained to understand Sb speciation and its interaction with soil components during ageing. XANES spectra were collected at the Materials Research Collaborative Access Team's (MRCAT) beamline 10-BM (Kropf et al., 2010) at the Advanced Photon Source (7 GeV storage ring in top-up mode), Argonne National Laboratory, Argonne, IL (USA). Soil samples, collected at different ageing times (i.e., 1, 31, 700 d), were prepared by freeze drying, grinding with an agate mortar and pestle, and pressing 75 mg of the sample in a 7-mm handheld pellet press. Samples from 7 and 91 d were not included in XANES analysis since SEP, DGT and SBRC data from these time-points were similar to those at 31 and 700 d respectively. The sample pellet was then encapsulated with Kapton tape and placed on a sample holder for analysis. The beamline optics and setup parameters for the Sb edge XANES measurements included calibration of the monochromator with a metallic Sb foil (30491 eV) and the acquisition of metallic foil spectra with each sample scan for spectral calibration verification. Data collection was conducted in both transmission and fluorescence (4-element Vortex Si-drift detector) modes with gas purged ion chambers for I_0 (80% Ar/20% N_2), $I_{Transmission}$ (100% Ar), and $I_{Reference}$ (100% Ar). At least six scans for each sample were collected and it was evident fluorescence data were of higher quality than transmission. Data analysis was conducted using Athena

software (Ravel and Newville, 2005). Multiple scans for each sample were aligned, merged, normalized, and calibration was performed by assigning the first inflection point of the reference Sb metal foil to 30491 eV. The relative abundance of Sb-bearing solid-phases was examined by linear combination fitting (LCF) of Sb K-edge XANES derivative spectra relative to known Sb reference samples (fitting range of -30 eV to +70 eV relative to the calibration energy). The χ^2 is a measure of the mean square sum of misfit at each data point and describes the degree of uncertainty in the fitting process (Ravel and Newville, 2005). Antimony reference standards included Sb_2S_3, Sb_2O_3, Sb(V)-tartrate, Sb(V)-citrate and $KSb(OH)_6$ (Sigma Aldrich, used for spike); Sb(V) and Sb(III) sorbed to goethite and Sb(III) sorbed to thiol-functionalised cellulose. Reference standards considered for LCF included Sb(V) sorbed to goethite to represent Sb(V) sorption by inorganic oxy-hydroxides (Essington and Stewart, 2018), Sb(V)-citrate to represent Sb(V) bound to organic matter, and $KSb(OH)_6$ to represent labile (e.g. water-soluble and exchangeable) Sb(V) in soil (Essington and Stewart, 2016). This latter interpretation was based on the high similarity of $KSb(OH)_6$ and $Sb(OH)_6^-$ spectra (e.g. Ji et al., 2017).

2.6. Statistical analysis

All chemical analyses were performed on triplicate soil samples collected from each mesocosm at different ageing times with mean values ± standard errors reported in tables and figures. The Shapiro-Wilk test was performed in order to evaluate the normality of data distribution. For each soil (S1 or S2) and contamination level (100 or 1000 $mg \cdot kg^{-1}$), the Fisher's LSD test was used to assess the influence of ageing

time on Sb mobility, potential bioavailability and bioaccessibility. Moreover, for each ageing time, comparisons between S1 and S2 at the same contamination level were made by using a Student t-test. Differences were considered statistically significant for $P < 0.05$. Pearson's correlation test was also performed to investigate the relationships between Sb concentrations recovered in the different steps of the SEP procedure, and those detected by DGT (i.e. C_{DGT}) at different ageing times. Correlation values were considered statistically significant for $P < 0.05$. All statistical analyses were carried out using the Sigma Plot Software (SPSS Inc., Chicago, IL, USA).

3. Results and discussion

3.1. Influence of ageing on Sb mobility in contaminated soils

To investigate the influence of ageing on the mobility of antimony in contaminated soils, different Sb fractions (or pools) characterised by a diverse degree of lability (i.e., solubility) were quantified at different time points. The water-soluble (i.e., highly mobile) Sb fraction (F1) decreased significantly over time for both soils and at both Sb concentrations (Fig. 1). The highest amounts of soluble Sb were detected at 1 d since spiking (40 and 18 % of total Sb for S1-100 and S2-100 and 24 and 26 % for S1-1000 and S2-1000 respectively), as previously reported elsewhere for other PTEs (e.g. Pb, Cu, Zn, Cd) (Jalali and Khanlari, 2008; Tang et al., 2006). Overall, such Sb amounts progressively and significantly reduced with ageing in both soils, even if different trends were observed depending on soil type and level of

contamination. In particular, significant reductions in water-soluble Sb occurred in all soils (with the exception of S2-100), after 7 d of ageing (Fig. 1). Interestingly, in S2-100, a significant reduction in soluble Sb occurred only at 91 d (Fig. 1). Such prolonged environmental stress could have favoured the development of an Sb-resistant bacterial community previously observed in this soil at 31 d ageing (Diquattro et al., 2020). The lowest amounts of soluble Sb were detected at 700 d of ageing even if, within each soil, the differences between 91 and 700 d were limited and, in some cases, not significant (Fig. 1). After 700 d ageing, soluble Sb was significantly reduced, compared to 1 d, by approx. 80 % in S1- and S2-100, and by 70 and 95 % in S1- and S2-1000 respectively. Taken together, these data indicate that 3 months ageing could be a suitable time for soil to equilibrate with aqueous Sb (i.e. very limited changes occurred after this time) and, consequently, to investigate the environmental fate of the contaminant and its ecotoxicological effects. Moreover, the higher Sb solubility observed in S1 compared with S2, especially after 700 d ageing (6 and 77 $mg \cdot kg^{-1}$ in S1-100 and -1000 vs 4 and 13 $mg \cdot kg^{-1}$ in S2-100 and -1000), could support previous research findings (Diquattro et al., 2020; Herath et al., 2017) where pH was identified as a key factor influencing Sb mobility. In particular, competition phenomena between hydroxide (OH^-) and $Sb(OH)_6^-$ anions for Sb retention sites and/or repulsion between $Sb(OH)_6^-$ anions and negatively charged soil surfaces, could explain the higher Sb solubility in the alkaline S1 soil (pH 8.2) compared to the acidic S2 (pH 4.9). On the contrary, Fe/Al oxides and soil organic matter, i.e. other important sinks of soil Sb (Herath et al., 2017), seemed to play a limited or negligible role at influencing Sb mobility in these soils (Fe/Al content was much higher in S1, and SOM content was similar in S1 and S2).

After 1 d ageing, Sb extracted with $(NH_4)_2SO_4$ (F2), i.e. the exchangeable pool, was significantly lower than water-soluble Sb in both soils (Fig. 1). Moreover, Sb extracted in F2 was significantly higher in S1-100 and -1000 (15.4 and 13.7 %) compared to S2-100 and -1000 (8.4 and 8.6 %), in agreement with the results of a recent short-term investigation based on the same soils (Fig. 1; Diquattro et al., 2020). Starting from 7 or 31 d, the amounts of exchangeable Sb significantly and progressively decreased (compared to 1 d) in all soils except S2-100 where a reduction was observed only at 700 d ageing (Fig. 1). Overall these data indicate a decrease of weaker (e.g. outer sphere) complexes and a concomitant increase of more specific (e.g. inner sphere) bonding between Sb and soil mineral and organic surfaces over time (Violante et al., 2010; Wenzel et al., 2001). As for the water-soluble F1 fraction, this implied a Sb shift from more mobile (and potentially bioavailable) pools to less mobile (and hardly bioavailable) ones during ageing.

This was partly supported by Sb extracted with $NH_4H_2PO_4$ (F3), i.e. Sb specifically sorbed by soil colloids (Wenzel et al., 2001). Such Sb pool can be considered as relatively mobile since it can be mobilised following a local pH change and/or a variation in P concentration (Wenzel et al., 2001). Antimony extracted in F3 was generally low at day 1 (i.e., 10.2 and 7.6 % of total Sb for S1-100 and -1000, and 3.7 and 2.3 % for S2-100 and -1000 respectively) which reduced (e.g. S1-100 and S2-1000) or remained constant (e.g. S1-100) during ageing (Fig. 1). The only exception was S1-1000 where Sb concentration slightly (yet significantly) increased with time, i.e. from 76 (at 1 d) to 81 $mg \cdot kg^{-1}$ soil (at 700 d) (Fig. 1).

Antimony detected in F4, i.e. residual Sb (e.g. associated with amorphous and crystalline Al and Fe oxy-hydroxides and/or precipitated or occluded), significantly

increased over time from 34, 70, 55 and 63 % at 1 d to 82, 79, 88 and 95 % at 700 d ageing in S1- and S2-100, and S1- and S2-1000 respectively (Fig. 1). This was in agreement with previous studies (e.g. Jalali and Khanlari, 2008; Peng et al., 2019) which reported an increase in residual PTEs such as Se, Pb, Cu, Cd, and Zn with ageing. However, the influence of ageing on Sb fractionation has been rarely addressed (e.g. Egodawatta et al., 2018; Zhang et al., 2020).

Taken together, SEP results highlighted a re-distribution of Sb from soluble (i.e., mobile) or weakly bound (easily mobilizable) forms, to less mobile and more stable ones during ageing. From an environmental viewpoint, this implies a time-dependent decrease in (micro)biological-impacting Sb fractions and an increase in less bioavailable forms.

3.2. Influence of ageing on Sb bioavailability in contaminated soils

The diffusive gradient in thin film technique (DGT) was used to measure the flux of soluble Sb, which is supplied by diffusion through soil solution, as well as that of labile Sb resupplied by the soil solid phase to the DGT device (Letho, 2016). The diffusion of labile soil Sb (free and complexed soluble ions and weakly bound Sb species) into DGT devices has been previously shown to mimic the continuous uptake of PTEs by plant roots (Zhou et al., 2019). This is because, as pointed out by Zhang and Davison (2000), elemental flux to plant membranes and to DGT can be similar from a quantitative viewpoint (Letho et al., 2016). For this reason, the use of the DGT technique to estimate PTEs bioavailability to plants and soil (micro)biota has been steadily growing (e.g. Dai et al., 2018; Gu et al., 2017; Wang et al., 2019).

The C_{DGT} measurements showed that bioavailable Sb rapidly decreased at the initial stage of ageing (7-31 d) and reached an equilibrium at 91 d (in agreement with SEP results) in the majority of soils (Fig. 2). At low contamination levels (i.e., 100 $mg \cdot kg^{-1}$), Sb bioavailability was always higher for soil S2 at all ageing times. However, after 700 d ageing, Sb-C_{DGT} values in the pore water of the two soils were low and similar, i.e. 0.33 and 0.49 $\mu g \cdot L^{-1}$ (Fig. 2). This is relevant, as these concentrations are expected to pose limited threats for plants and soil (micro)biota (Geng et al., 2020; Sh et al., 2012). Nonetheless, it should be noted that much higher Sb-C_{DGT} concentrations were detected during the previous time-points and this could have produced substantial perturbations of soil (micro)biological and biochemical features (e.g. Diquattro et al., 2020) whose effects could be still present after 700 d. In soils containing higher Sb concentrations (i.e., 1000 $mg \cdot kg^{-1}$), Sb bioavailability was significantly higher for soil S1 at all ageing times, with the exception of day 1 (Fig. 2). After 700 d ageing, the Sb-C_{DGT} in S1 was still 4.5-fold higher than in S2, and this supports higher Sb mobility detected by the SEP procedure in soil S1 (Fig. 1). As previously mentioned, this could be attributed to the alkaline pH of soil S1 and/or to the increased formation of stable Sb precipitates (e.g. $FeSbO_4$ and $AlSbO_4$) in the acidic S2 (Dousova et al., 2018; Herath et al., 2017). It should be noted that, at low Sb contamination level (i.e., 100 $mg \cdot kg^{-1}$), this was not particularly evident as highlighted by both SEP and DGT results (Figs. 1-2). Overall, these results clearly indicate a steady reduction in Sb bioavailability during ageing, which also suggests a parallel increase in stable Sb-soil interactions over time, which was supported by SEP results.

The resupply of Sb from the solid phase to the soil pore water, i.e. R value (C_{DGT} / C_{sol}), was low in both soils for all ageing times (i.e., R < 0.12 and < 0.05 for S-100 and S-1000 soils; Table 2) indicating that diffusion was the main process supplying Sb to the DGT device (Ma et al., 2020; Netho, 2016; Peng et al., 2019). Since the selected Sb fractions extracted by SEP are often correlated with the most labile (and potentially bioavailable) fractions in soil, i.e. those readily taken up by plants and soil microorganisms (e.g. Castaldi et al., 2018; Diquattro et al., 2018, 2020; Garau et al., 2017), the correlation between Sb-C_{DGT} and that recovered in F1-F4 was tested (Table 3). Significant positive correlations were observed between F1 (0.786 – 0.959; $P < 0.01$), and F1+F2 (0.683 – 0.979; $P < 0.01$), and Sb-C_{DGT} while weaker relationships were recorded for F2 (Table 3). No significant relationship between Sb-C_{DGT} and F3 was found, whereas significant negative correlations were observed between F4 (i.e., the less mobile and less bioavailable Sb) and Sb-C_{DGT} (Table 3).

Taken together, these data highlight a good agreement between DGT and SEP results and confirmed the suitability of both approaches for the assessment of Sb mobility and potential bioavailability in soil. Overall, Sb-C_{DGT} values showed that ageing had a marked influence on the potential bioavailability of Sb. This latter steadily decreased with time due to the conversion of Sb labile fractions into non-labile ones as indicated by SEP results.

3.3. Influence of ageing on Sb bioaccessibility

To investigate the influence of ageing on potential exposure for humans and animals related to incidental ingestion of Sb-contaminated soil, gastric and intestinal

phase Sb bioaccessibility was determined at different ageing times using the in vitro SBRC assay. Antimony bioaccessibility varied over time, and different trends were observed depending on soil type and Sb concentration (Fig. 3). When assessed using SBRC-G, Sb bioaccessibility significantly decreased with increasing ageing times with the exception of S1-100 when no variation in Sb bioaccessibility was recorded (Fig. 3). After 700 d ageing, Sb bioaccessibility in the SBRC-G phase was ~30, 26, 39 and 9 % (of total Sb present in the < 250 μm soil fractions) in S1- and S2-100, and S1- and S2-1000 respectively.

Considering that elemental absorption takes place in the intestinal compartment (Hamel et al., 1998), SBRC-I data are of particular interest. Antimony bioaccessibility in the SBRC-I phase quickly declined with ageing in the majority of soils (Fig. 3). In particular, significant reductions in bioaccessible Sb were recorded after 7 d for S2-1000 and after 31 d for S2-100 and S1-1000. However, it should be noted that after one day, Sb bioaccessibility in the SBRC-I phase was 46 % (of total Sb present in the < 250 μm soil fraction; Table 1) in S1-100 and between 61 and 72 % in the remaining soils (Fig. 3), that means an approx. 55 – 1800 mg $Sb \cdot kg^{-1}$ soil. Nonetheless, ageing had a clear influence on Sb bioaccessibility (SBRC-I) which declined, compared to day 1, by a minimum of 15 % in S1-100, up to 60 % in S2-1000 (Fig. 3). Again, this supports a time-dependent increase of stable bonds between Sb and soil components (e.g. Fe oxy-hydroxides and organic matter), able to resist dissolution processes which take place during digestion (Denys et al., 2008). However, this was more pronounced for S2 soils where Sb binding to Fe/Al oxy-hydroxides and organic matter was likely favoured by the lower pH. Indeed, the acidic pH of the gastric phase commonly promotes the solubilisation of mineral

phases and the release of bonded PTEs, while the higher concentration of OH^- in the intestinal phase can prevent anion sorption/adsorption [e.g. $Sb(OH)_6^-$] by soil colloids which favours the release of further Sb into solution (Udovic and Mcbride, 2012).

Even if these results indicate a decreased Sb bioaccessibility over time, nonetheless, absolute Sb concentrations recorded in the SRBC-I phase at 700 d (i.e., 43 and 511 $mg \cdot kg^{-1}$ for S1-100 and S1-1000 respectively, and 90 and 367 $mg \cdot kg^{-1}$ for S2-100 and S2-1000) highlighted substantial potential health risks in both contaminated soils (Filella et al., 2002).

3.4. Influence of ageing on Sb speciation

Biogeochemical redox processes strongly influence Sb speciation, its interactions with soil colloids (and hence mobility and stability) as well as its toxicity. In this sense, spectroscopic techniques such as electron spin resonance (ESR) and X-ray absorption spectroscopy (XAS, including XANES) have been useful for the identification of metal and metalloid speciation and their complexes at surfaces of Al, Fe or Mn oxy-hydroxides, silicate clays and soil organic matter (Violante et al., 2010).

Derivative XANES spectra of Sb reference materials considered for LCF and of S1 and S2 soils are shown in Fig.s S1 and S2 respectively. LCF results for S1 and S2 samples (Table 4, Fig. S2) show the presence of labile Sb(V) (i.e. $KSb(OH)_6$ spectra) at varying degrees. Importantly, Sb(V) was the only redox state identified in XANES data. Labile Sb(V) concentration was higher for S1 samples than S2. Again, this

503 could be due to the influence of pH (8.2 vs 4.9, respectively) given the similar SOM
504 content of S1 and S2 (1.75 and 2.19 %), and the higher Fe and Al content in the
505 former soil (~ 3 and 5-fold respectively compared to S2). A similar influence of pH
506 on Sb sorption by ferrihydrite was recently reported by Garau et al. (2019).
507 Consistently, higher Sb-organic interactions (Sb(V)-citrate) and Sb sorbed to
508 inorganic oxides (Sb(V)-goethite LCF reference) were recorded in S2 relative to S1
509 over time (Table 4). XANES spectroscopy is often not sensitive enough to
510 distinguish if elements are sorbed by Fe or Al oxy-hydroxides in a complex soil
511 matrix; however, spectra obtained are unique enough to distinguish them from
512 organic complexes.
513 The initial concentration of Sb in each soil influenced final speciation results. S1-
514 100 at 700 d resulted in Sb speciation components of 57 % $KSb(OH)_6$ (which is
515 indicative of labile $Sb(OH)_6^-$), 18 % organic bound Sb(V), and 24 % sorbed to
516 inorganic oxides; whereas S1-1000 at 700 d observed 81 % $KSb(OH)_6$, 14 % organic
517 bound Sb(V), and 5 % sorbed to inorganic oxides. A similar trend was noted for the
518 S2 concentration series where the $KSb(OH)_6$ fraction was larger for the higher
519 concentrated spiked sample.
520
521 **4. Conclusions**
522
523 Ageing had a clear influence on Sb mobility, bioavailability and bioaccessibility
524 in contaminated soils. Labile (i.e., more soluble) Sb fractions progressively reduced
525 during ageing indicating a decrease of weaker (e.g. outer-sphere) complexes and a
526 concomitant increase of more specific (e.g. inner-sphere) bonding between Sb and

the soil components over time. This was accompanied by a parallel decrease of bioavailable and bioaccessible Sb which implied: i) a time-dependent increase of stable bonding between Sb and soil components and ii) a reduced ecotoxicological Sb impact on soil (micro)biota and humans with ageing. XANES LCF results indicated that Sb(V) was the only redox state present in soils during the almost 2-years experiment and that soil organic matter and Fe/Al oxy-hydroxides were the main sink of Sb during ageing. In this regard, soil pH appeared as a key parameter influencing the fate of Sb in our soils, i.e. Sb mobility, bioavailability and bioaccessibility were overall higher in the alkaline S1 soil compared to the acidic S2. Consistently, Sb fixation by soil organic matter and Fe/Al oxy-hydroxides was quantitatively less in S1 compared with S2 at all time-points considered. Nevertheless, absolute Sb concentrations recorded in the intestinal phase at 700 d highlight substantial potential health risks in both contaminated soils.

Credit Author Statement

Stefania Diquattro: Investigation, Methodology, Formal analysis, Writing - Original draft preparation. **Paola Castaldi:** Conceptualization, Formal analysis, Resources, Writing - Review & Editing. **Susie Ritch:** Methodology. **Albert L. Juhasz:** Resources, Formal analysis. **Gianluca Brunetti:** Methodology. **Kirk G. Scheckel:** Investigation, Formal analysis, Methodology, Writing - Review & Editing. **Giovanni Garau:** Conceptualization, Formal analysis, Writing - Review & Editing. **Enzo Lombi:** Conceptualization, Resources, Writing - Review & Editing, Project administration.

Acknowledgements

The financial support of the University of Sassari (Fondo di Ateneo per la Ricerca 2019) is gratefully acknowledged.

MRCAT operations are supported by the Department of Energy and the MRCAT member institutions. This research used resources of the Advanced Photon Source, a U.S. Department of Energy (DOE) Office of Science User Facility operated for the DOE Office of Science by Argonne National Laboratory under Contract No. DE-AC02-06CH11357. Although EPA contributed to this article, the research presented was not performed by or funded by EPA and was not subject to EPA's quality system requirements. Consequently, the views, interpretations, and conclusions expressed in this article are solely those of the authors and do not necessarily reflect or represent EPA's views or policies.

The Future Industries Institute, University of South Australia is acknowledged for supporting this project.

Appendix A. Supplementary data.

Supplementary material related to this article is supplied as Table S1, Fig.s S1 and S2.

References

Bagherifam, S., Lakzian, A., Fotovat, A., Khorasani, R., Komarneni, S., 2014. In situ stabilization of As and Sb with naturally occurring Mn, Al and Fe oxides in a calcareous soil: Bioaccessibility, bioavailability and speciation studies. J. Hazard. Mater. 273, 247–252.

Castaldi, P., Diquattro, S., Lauro, G.P., Marceddu, S., Garau, G., 2018. Water treatment residuals as a resource for the recovery of soil and water polluted with Sb(V): sorption and desorption trials at different pH values. Water Air Soil Pollut. 229(6), 174.

CEC, 1998. Council Directive 98/83/EC of 3 November 1998 on the quality of water intended for human consumption (OJ L 330 05.12.1998 p. 32). In: Sands, P., Galizzi, P. (Eds.), Documents in European Community Environmental Law. Cambridge University Press, Cambridge, pp. 865–878.

Courtin-Nomade, A., Rakotoarisoa, O., Bril, H., Grybos, M., Forestier, L., Foucher, F., Kunz, M., 2012. Weathering of Sb-rich mining and smelting residues: insight in solid speciation and soil bacteria toxicity. Chem. Erde-Geochem. 72, 29–39.

Dai, Y., Nasir, M., Zhang, Y., Gao, J., Lv, Y., Lv, J., 2018. Comparison of DGT with traditional extraction methods for assessing arsenic bioavailability to *Brassica chinensis* in different soils. Chemosphere 191, 183–189.

Davison, W., Zhang, H., 1994. In situ speciation measurements of trace components in natural waters using thin-flm gels. Nature 367, 546–548.

Denys, S., Tack, K., Caboche, J., Delalain, P., 2008. Bioaccessibility, solid phase distribution, and speciation of Sb in soils and in digestive fluids. Chemosphere 74, 711–716.

Diagboya, P.N., Olu-Owolabi, B.I., Adebowale, K.O., 2015. Effects of aging, soil organic matter, and iron oxides on the relative retention of lead, cadmium, and copper on soils. Environ. Sci. Pollut. Res. 22, 10331–10339.

Diquattro, S., Garau, G., Lauro, G.P., Silvetti, M., Deiana, S., Castaldi, P., 2018. Municipal solid waste compost as a novel sorbent for antimony(V): adsorption and release trials at acidic pH. Environ. Sci. Pollut. Res. 25, 5603–5615.

Diquattro, S., Garau, G., Mangia, N.P., Drigo, B., Lombi, E., Vasileiadis, S., Castaldi, P., 2020. Mobility and potential bioavailability of antimony in contaminated soils: Short-term impact on microbial community and soil biochemical functioning. Ecotoxicol. Environ. Safe. 196, 110576.

Dousova, B., Lhotka, M., Filip, J., Kolousek, D., 2018. Removal of arsenate and antimonate by acid-treated Fe-rich clays. J. Hazard. Mater. 357, 440–448.

Egodawatta, L.P., Macoustra, G.K., Ngo, L.K., Jolley, D.F., 2018. As and Sb are more labile and toxic to water spinach (*Ipomoea aquatica*) in recently contaminated soils than historically co-contaminated soils. Environ. Sci. Proc. Imp. 20, 833–844.

Essington, M.E., Stewart, M.A., 2016. Adsorption of antimonate by gibbsite: Reversibility and the competitive effects of phosphate and sulfate. Soil Science Society of America Journal 80, 1197–1207.

Essington, M.E., Stewart, M.A., 2018. Adsorption of antimonate, sulfate, and phosphate by goethite: Reversibility and competitive effects. Soil Science Society of America Journal 82, 803–814.

Filella, M., Belzile, N., Chen, Y.W., 2002. Antimony in the environment: A review focused on natural waters I. Occurence. Earth-Sci. Rev. 57, 125–176.

Filella, M., Williams, P.A., Belzile, N., 2009. Antimony in the environment: Knowns and unknowns. Environ. Chem. 6, 95–105.

Garau, G., Silvetti, M., Vasileiadis, S., Donner, E., Diquattro, S., Deiana, S., Lombi, E., Castaldi, P., 2017. Use of municipal solid wastes for chemical and microbiological recovery of soils contaminated with metal(loid)s. Soil Biol. Biochem. 111, 25–35.

Garau, G., Lauro, G.P., Diquattro, S., Garau, M., Castaldi, P., 2019. Sb(V) adsorption and desorption onto ferrihydrite: influence of pH and competing organic and inorganic anions. Environ. Sci. Pollut. Res. 26, 27268–27280.

Geng, L, Yang, Z., Xu, Z., 2020. Effects of antimony contamination in soil on the nutrient composition of three green leafy vegetables. Journal Soil. Sediment. 20, 2217–2224.

Gu, X., Liu, Z., Wang, X., Luo, J., Zhang, H., Davison, W., Ma, L.Q., Xue, Y., 2017. Coupling biological assays with diffusive gradients in thin-films technique to study the biological responses of *Eisenia fetida* to cadmium in soil. J. Hazard.

636 Mater. 339, .340–346.
637 Hamel, S.C., Buckley, B., Lioy, P.J., 1998. Bioaccessibility of metals in soils for
638 different liquid to solid ratios in synthetic gastric fluid. Environ. Sci. Technol.
639 32, 358–362.
640 Hammel, W., Debus, R., Steubing, L., 2000. Mobility of antimony in soil and its
641 availability to plants. Chemosphere 41, 1791–1798.
642 Harper, M.P., Davison, W., Tych, W., 2000. DIFS - a modelling and simulation tool
643 for DGT induced trace metal remobilisation in sediments and soils. Environ.
644 Model. Softw. 15, 55–66.
645 He, M., Wang, N., Long, X., Zhang, C., Ma, C., Zhong, Q., Wang, A., Wang, Y.,
646 Pervaiz, A., Shan, J., 2019. Antimony speciation in the environment: Recent
647 advances in understanding the biogeochemical processes and ecological effects.
648 J. Environ. Sci. (China) 75, 14–39.
649 Herath, I., Vithanage, M., Bundschuh, J., 2017. Antimony as a global dilemma:
650 Geochemistry, mobility, fate and transport. Environ. Pollut. 223, 545–559.
651 Jalali, M., Khanlari, Z.V., 2008. Effect of aging process on the fractionation of heavy
652 metals in some calcareous soils of Iran. Geoderma 143, 26–40.
653 Ji, Y., Sarret, G., Schulin, R., Tandy, S., 2017. Fate and chemical speciation of
654 antimony (Sb) during uptake, translocation and storage by rye grass using
655 XANES spectroscopy. Environmental Pollution 231, 1322–1329.
656 Johnston, S.G., Bennett, W.W., Doriean, N., Hockmann, K., Karimian, N., Burton,
657 E.D., 2020. Antimony and arsenic speciation, redox-cycling and contrasting
658 mobility in a mining-impacted river system. Sci. Total Environ. 710, 136354.
659 Jury, W., Gardner, W.R., Gardner, W.H. 1991. Soil Physics. 5th ed. John Wiley &
660 Sons, New York.
661 Kang, M., Kawasaki, M., Tamada, S., Kamei, T., Magara, Y., 2000. Effect of pH on
662 the removal of arsenic and antimony using reverse osmosis membranes.
663 Desalination 131, 293–298.
664 Kropf, A.J., Katsoudas, J., Chattopadhyay, S., Shibata, T., Lang, E.A., Zyryanov,
665 V.N., Ravel, B., McIvor, K., Kemner, K.M., Scheckel, K.G., Bare, S.R., Terry,
666 J., Kelly, S.D., Bunker, B.A., Segre, C.U., 2010. The new MRCAT (Sector 10)
667 Bending Magnet beamline at the Advanced Photon Source. AIP Conference

668 Proceedings 1234, 299–302.
669 Letho, N.J., 2016. Principles and application in soils and sediments. In: Davison, W.
670 (Ed.), Diffusive gradients in thin-films for environmental measurements.
671 Cambridge University Press, Padstow (United Kingdom), pp. 146–173.
672 Li, C., Ding, S., Yang, L., Wang, Y., Ren, M., Chen, M., Fan, X., Lichtfouse, E.,
673 2018. Diffusive gradients in thin films: devices, materials and applications.
674 Environ. Chem. Lett. 17, 801–831.
675 Li, J., Wei, Y., Zhao, L., Zhang, J., Shangguan, Y., Li, F., Hou, H., 2014.
676 Bioaccessibility of antimony and arsenic in highly polluted soils of the mine
677 area and health risk assessment associated with oral ingestion exposure.
678 Ecotoxicol. Environ. Safe. 110, 308–315.
679 Luo, J., Bai, Y., Liang, J., Qu, J., 2014. Metagenomic approach reveals variation of
680 microbes with arsenic and antimony metabolism genes from highly
681 contaminated soil. PLoS One 9.
682 Luo, J., Zhang, H., Santner, J., Davison, W., 2010. Performance characteristics of
683 diffusive gradients in thin films equipped with a binding gel layer containing
684 precipitated ferrihydrite for measuring Arsenic(V), Selenium(VI),
685 Vanadium(V), and Antimony(V). Anal. Chem. 82, 8903–8909.
686 Ma, X., Li, C., Yang, L., Ding, S., Zhang, M., Zhang, Y., Zhao, T., 2020. Evaluating
687 the mobility and labile of As and Sb using diffusive gradients in thin-films
688 (DGT) in the sediments of Nansi Lake, China. Sci. Total Environ. 713, 136569.
689 Maher, W.A., Krikowa, F., Foster, S.D., Ellwood, M.J., Bennett, W.W., 2018.
690 Antimony measurements in environmental matrices: Seven considerations. J.
691 Anal. At. Spectrom. 33, 706–712.
692 Martínez, C.E., McBride, M.B., 2001. Cd, Cu, Pb, and Zn coprecipitates in Fe oxide
693 formed at different pH: Aging effects on metal solubility and extractability by
694 citrate. Environ. Toxicol. Chem. 20, 122–126.
695 Mele, E., Donner, E., Juhasz, A.L., Brunetti, G., Smith, E., Betts, A.R., Castaldi, P.,
696 Deiana, S., Scheckel, K.G., Lombi, E., 2015. In situ fixation of metal(loid)s in
697 contaminated soils: a comparison of conventional, opportunistic, and engineered
698 soil amendments. Environ. Sci. Technol. 49, 13501–13509.
699 Ngo, L.K., Price, H., Bennet, W.W., Teasdale, P.R., Jolley, D.F., 2020. DGT and

selective extractions reveal differences in arsenic and antimony uptake by the white icicle radish (*Raphanus sativus*). Environ. Pollut. 259, 113815.

Okkenhaug, G., Grasshorn Gebhardt, K.A., Amstaetter, K., Lassen Bue, H., Herzel, H., Mariussen, E., Rossebø Almås, Å., Cornelissen, G., Breedveld, G.D., Rasmussen, G., Mulder, J., 2016. Antimony (Sb) and lead (Pb) in contaminated shooting range soils: Sb and Pb mobility and immobilization by iron based sorbents, a field study. J. Hazard. Mater. 307, 336–343.

Peng, Q., Li, J., Wang, D., Wei, T.J., Chen, C.E.L., Liang, D.L., 2019. Effects of ageing on bioavailability of selenium in soils assessed by diffusive gradients in thin-films and sequential extraction. Plant Soil 436, 159–171.

Ravel, B., Newville, M., 2005. ATHENA, ARTEMIS, HEPHAESTUS: data analysis for X-ray absorption spectroscopy using IFEFFIT. J. Synchrotron Radiat. 12, 537–541.

Ruby, M.V., Davis, A., Schoof, R., Eberle, S., Sellstone, C.M., 1996. Estimation of lead and arsenic bioavailability using a physiologically based extraction test. Environ. Sci. Technol. 30, 422–430.

Sanderson, P., Naidu, R., Bolan, N., 2014 Ecotoxicity of chemically stabilised metal(loid)s in shooting range soils. Ecotoxicol. Environ. Safe. 100, 201–208.

Sh, T., Liu, C.Q., Wang, L., 2012. Antimony coordination to humic acid: Nuclear magnetic resonance and X-ray absorption fine structure spectroscopy study. Microchem. J. 103, 68–73.

Steely, S., Amarasiriwardena, D., Xing, B., 2007. An investigation of inorganic antimony species and antimony associated with soil humic acid molar mass fractions in contaminated soils. Environ. Pollut. 148, 590–598.

Tang, X.Y., Zhu, Y.G., Cui, Y.S., Duan, J., Tang, L., 2006. The effect of ageing on the bioaccessibility and fractionation of cadmium in some typical soils of China. Environ. Int. 32, 682–689.

Tang, X.Y., Zhu, Y-G, Shan, X-Q., McLaren, R., Duan, J., 2007. The ageing effect on the bioaccessibility and fractionation of arsenic in soils from China. Chemosphere 66, 1183–1190.

Telford, K., Maher, W., Krikowa, F., Foster, S., 2008. Measurement of total antimony and antimony species in mine contaminated soils by ICPMS and

HPLC-ICPMS. J. Environ. Monit. 10, 136–140.

Tella, M., Pokrovski, G.S., 2009. Antimony(III) complexing with O-bearing organic ligands in aqueous solution: An X-ray absorption fine structure spectroscopy and solubility study. Geochim. Cosmochim. Acta 73, 268–290.

Tella, M., Pokrovski, G.S., 2012. Stability and structure of pentavalent antimony complexes with aqueous organic ligands. Chem. Geol. 292–293, 57–68.

Udovic, M., McBride, M.B., 2012. Influence of compost addition on lead and arsenic bioavailability in reclaimed orchard soil assessed using Porcellio scaber bioaccumulation test. J. Hazard. Mater. 205–206, 144–149.

USEPA, 2009. National Primary Drinking Water Regulations.

Violante, A., Cozzolino, V., Perelomov, L., Caporale, A.G., Pigna, M., 2010. Mobility and bioavailability of heavy metals and metalloids in soil environments. J. Soil Sci. Plant Nutr. 10, 268–292.

Yang J-K, Barnett M.O., Jardine P.M, Brooks S.C., 2003. Factors controlling the bioaccessibility of arsenic(V) and lead(II) in soil. Soil Sediment Contam. 12(2), 165–179.

Wang, P., Lombi, E., Sun, S., Scheckel, K.G., Malysheva, A., McKenna, B.A., Menzies, N.W., Zhao, F.J., Kopittke, P.M., 2017. Characterizing the uptake, accumulation and toxicity of silver sulfide nanoparticles in plants. Environ. Sci. Nano 4, 448–460.

Wang, M., Cui, Z., Xue, M., Peng, Q., Zhou, F., Wang, D., Dinh, Q.T., Liu, Y., Liang, D., 2019. Assessing the uptake of selenium from naturally enriched soils by maize (*Zea mays* L.) using diffusive gradients in thin-films technique (DGT) and traditional extractions. Sci. Total Environ. 689, 1–9.

Wenzel, W.W., Kirchbaumer, N., Prohaska, T., Stingeder, G., Lombi, E., Adriano, D.C., 2001. Arsenic fractionation in soils using an improved sequential extraction procedure. Anal. Chim. Acta 436, 309–323.

Wilson, S.C., Lockwood, P. V., Ashley, P.M., Tighe, M., 2010. The chemistry and behaviour of antimony in the soil environment with comparisons to arsenic: A critical review. Environ. Pollut. 158, 1169–1181.

Xi, J., He, M., Kong, L., 2016. Adsorption of antimony on kaolinite as a function of time, pH, HA and competitive anions. Environ. Earth Sci. 75, 1–7.

764 Zhang, H., Davison, W., 2000. Direct in situ measurements of labile inorganic and
765 organically bound metal species in synthetic solutions and natural waters using
766 diffusive gradients in thin films. Anal. Chem. 72, 4447.
767 Zhang, P., Wu, T.L., Ata-Ul-Karim, S.T., Ge, Y.Y., Cui, X., Zhou, D.M., Wang,
768 Y.J., 2020. Influence of soil properties and aging on antimony toxicity for
769 barley root elongation. B. Environ. Contam. Tox. 104, 714–720.
770 Zhou, J.W., Wu, L.H., Zhou, T., Li, Z., Sun, X.Y., Luo, Y.M., Christie P., 2019.
771 Comparing chemical extraction and a piecewise function with diffusive
772 gradients in thin films for accurate estimation of soil zinc bioavailability to
773 Sedum plumbizincicola. Eur. J. Soil Sci. 70, 1141–1152.
774

775 **Figure captions**

776

777 **Fig. 1.** Sequential extraction of antimony from S1 and S2 soils spiked with 100 (S-
778 100) and 1000 (S-1000) mg Sb kg^{-1} soil at different ageing time. For each Sb fraction
779 (F_x), different letters on top of each bar (e.g. a, b, c, d) denote ageing-dependent
780 statistical differences (Fisher's LSD, $P < 0.05$). For each Sb fraction and ageing time,
781 asterisks denote statistical differences between S1-100 and S2-100, and between S1-
782 1000 and S2-1000 soils (Student t-test, $P < 0.05$).

783

784 **Fig. 2.** Antimony concentrations as obtained by DGT (Sb-C_{DGT}) in S1 and S2 soils
785 spiked with 100 (S-100) and 1000 (S-1000) mg Sb kg^{-1} soil at different ageing time.
786 For each soil, different letters on top of each bar (e.g. a, b, c, d) denote ageing-
787 dependent statistical differences (Fisher's LSD, $P < 0.05$). For each ageing time,
788 asterisks denote statistical differences between S1-100 and S2-100, and between S1-
789 1000 and S2-1000 soils (Student t-test, $P < 0.05$).

790

791 **Fig. 3.** *In vitro* bioaccessibility of Sb in S1 and S2 soils spiked with 100 (S-100) and
792 1000 (S-1000) mg Sb kg^{-1} soil at different ageing time. For each soil, different letters
793 on top of each bar (e.g. a, b, c, d) denote ageing-dependent statistical differences
794 (Fisher's LSD, $P < 0.05$). For each ageing time, asterisks denote statistical
795 differences between S1-100 and S2-100, and between S1-1000 and S2-1000 soils
796 (Student t-test, $P < 0.05$). SBRC-G= bio-accessible Sb in the gastric phase; SBRC-I
797 = bio-accessible Sb in the intestinal phase.

798

Table S1. Selected physico-chemical characteristics of S1 and S2 soils.

Fig. S1. Derivative XANES spectra of antimony reference materials considered for linear combination fitting.

Fig. S2. Derivative XANES spectra of antimony from S1 and S2 soils spiked with 100 (S-100) and 1000 (S-1000) mg Sb kg^{-1} soil at different ageing time. Black curves represent sample data while red curves represent LCF results. Processed results are presented in Table 4.

Table 1

Concentration of total Sb in < 250 μm particle size fractions.

Time	Sb concentration (mg kg^{-1})	
	S1-100	*S1-1000*
1 d	121.1 ± 2.51	1167 ± 19.3
7 d	159.2 ± 6.86	1384 ± 9.64
31 d	119.0 ± 5.99	1326 ± 24.0
91 d	156.3 ± 1.65	1321 ± 22.3
700 d	139.0 ± 4.25	1403 ± 71.9
	S2-100	*S2-1000*
1 d	234.2 ± 9.13	2500 ± 47.2
7 d	237.9 ± 7.94	2954 ± 438
31 d	254.2 ± 1.21	2734 ± 250
91 d	297.0 ± 30.2	2950 ± 268
700 d	252.1 ± 5.80	2956 ± 287

Table 2

Concentration of Sb in soil solution (C_{sol}) and R values in soils during ageing.

Ageing time (d)	C_{sol} ($\mu g \cdot L^{-1}$)				R value ($R = C_{DGT}/C_{sol}$)			
	S1-100	S2-100	S1-1000	S2-1000	S1-100	S2-100	S1-1000	S2-1000
1	88.88	38.06	535.6	596.6	0.049	0.119	0.045	0.050
7	28.83	37.44	300.3	91.2	0.039	0.068	0.035	0.049
31	27.64	39.11	260.3	72.2	0.036	0.046	0.033	0.039
91	13.33	16.73	212.3	35.3	0.039	0.061	0.030	0.038
700	15.76	8.84	173.0	26.6	0.021	0.056	0.028	0.041

Table 3

Pearson correlation coefficients (r) between the Sb fractions detected by SEP and those quantified by DGT (C_{DGT}) in S1 and S2 soils [ǂ].

	S1-100	S1-1000	S2-100	S2-1000
	C_{DGT}	C_{DGT}	C_{DGT}	C_{DGT}
F1	0.959**	0.946**	0.786**	0.947**
F2	0.853**	0.911**	0.297^{NS}	0.780**
F1+F2	0.967**	0.979**	0.683**	0.966**
F3	0.425^{NS}	-0.106^{NS}	-0.041^{NS}	-0.032^{NS}
F4	-0.958**	-0.921**	-0.537*	-0.963**

[ǂ]NS not significant ($P > 0.05$);* statistically significant at $P < 0.05$; ** statistically significant at $P < 0.01$.

Table 4

Linear Combination Fitting (LCF)−XANES analysis of Sb speciation.

	Sb speciation distribution (%)			
	$KSb(OH)_6$	Sb(V)-Citrate	Sb(V)-Goethite	χ^2
S1-100 1 d	88	12	0	0.0059
S1-100 31 d	63	19	18	0.0242
S1-100 700 d	57	18	24	0.0063
S2-100 1 d	55	32	13	0.0088
S2-100 31 d	43	36	21	0.0150
S2-100 700 d	36	37	27	0.0091
S1-1000 1 d	88	12	0	0.0022
S1-1000 31 d	85	12	3	0.0021
S1-1000 700 d	81	14	5	0.0034
S2-1000 1 d	62	25	13	0.0037
S2-1000 31 d	59	23	18	0.0014
S2-1000 700 d	58	21	21	0.0543

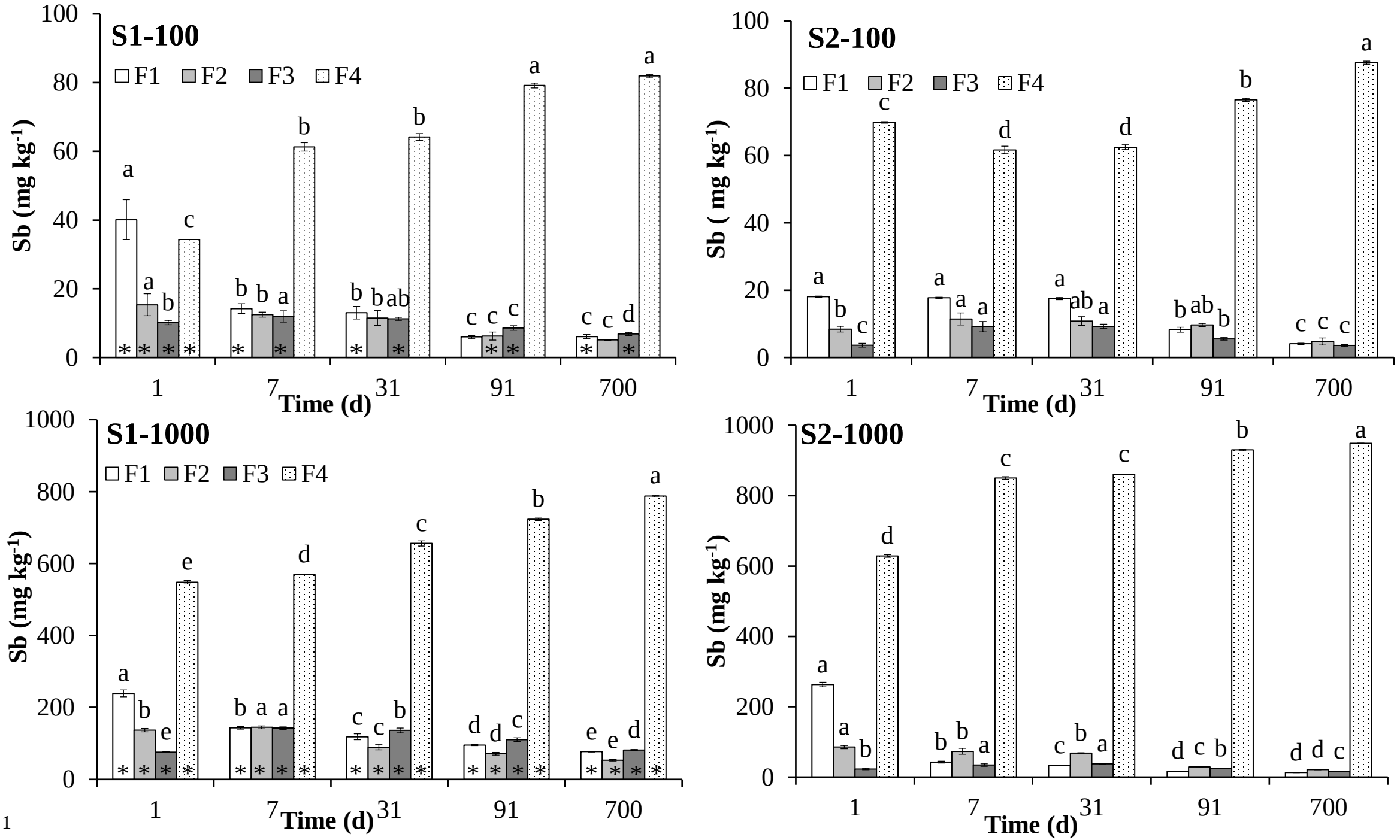
S1-100
F1 F2 F3 F4
Sb (mg kg-1)
Time (d)
1 7 31 91 700
S2-100
Sb (mg kg-1)
S1-1000
S2-1000

Figure 1

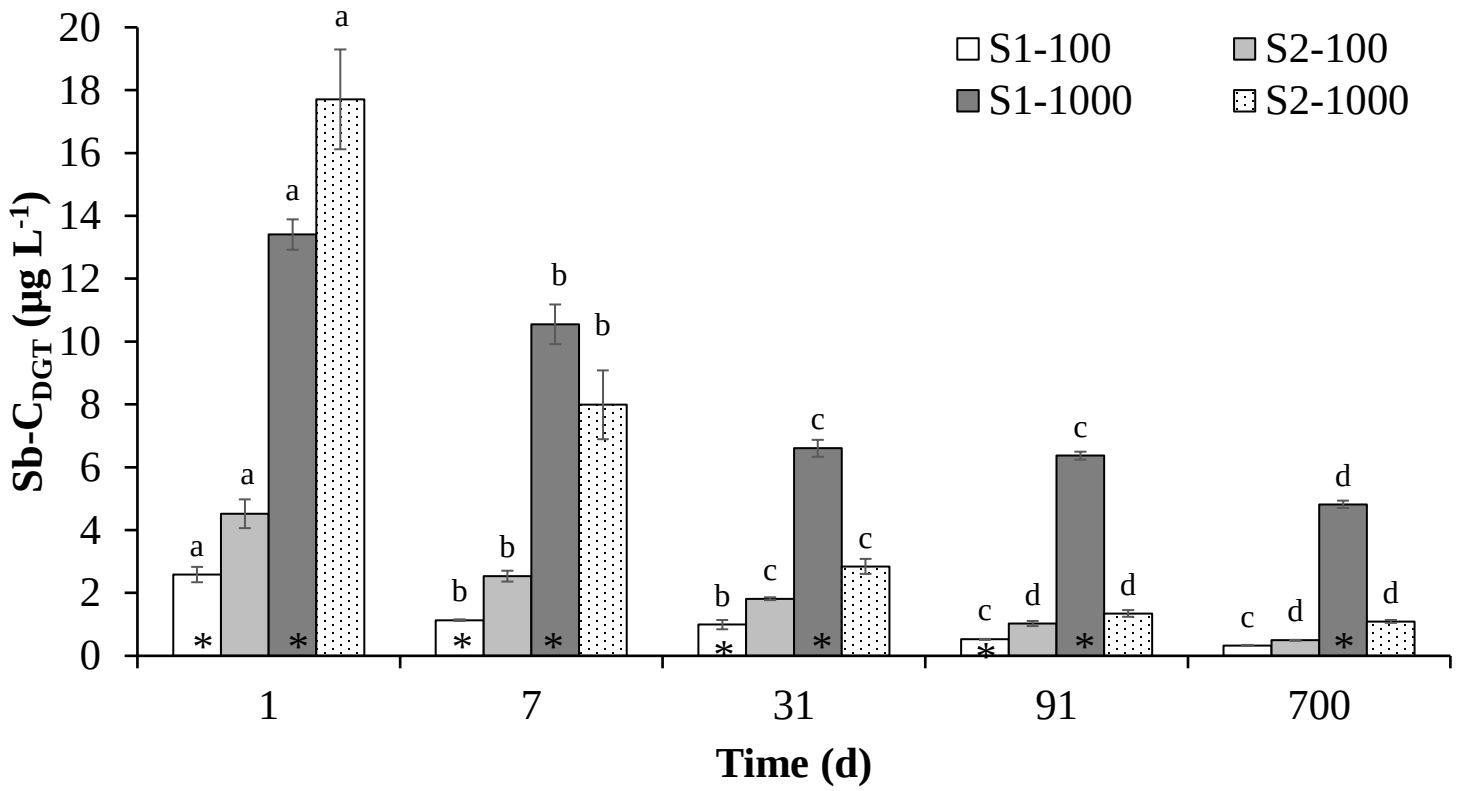
S1-100
S2-100
S1-1000
S2-1000
Sb-C$_{DGT}$ (µg L^{-1})
Time (d)
0
2
4
6
8
10
12
14
16
18
20
1
7
31
91
700
a
a
a
b
b
b
b
c
c
c
c
d
c
d
d
c
d
d
*

Figure 2

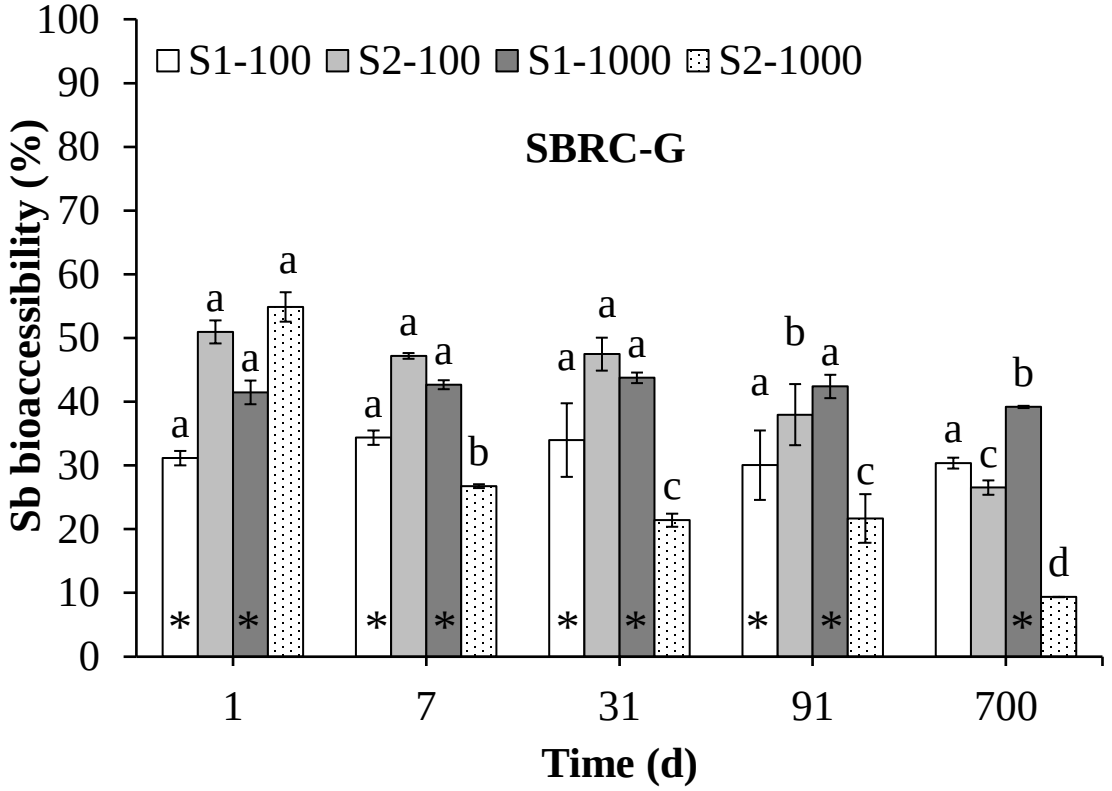
S1-100
S2-100
S1-1000
S2-1000
SBRC-G
Sb bioaccessibility (%)
Time (d)
1
7
31
91
700

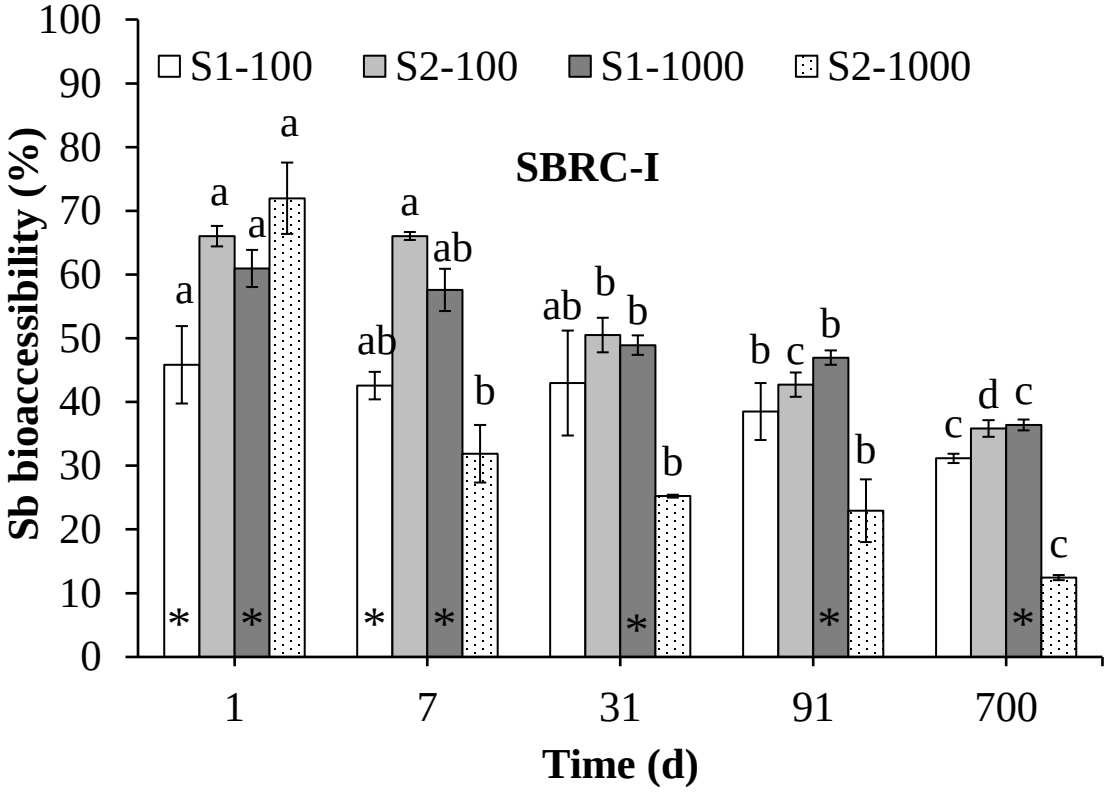
S1-100
S2-100
S1-1000
S2-1000
SBRC-I
Sb bioaccessibility (%)
Time (d)
1
7
31
91
700

Figure 3

Table S1. Selected physico-chemical characteristics of S1 and S2 soils.

Physico-chemical parameters	**S1 soil**	**S2 soil**
$pH_{(H_2O)}$	8.2 ± 0.1	4.9 ± 0.2
DOC (mg g^{-1})	0.17 ± 0.00	0.39 ± 0.02
SOM (%)	1.75 ± 0.1	2.19 ± 0.2
CEC ($cmol_{(+)}$ kg^{-1})	20 ± 0.8	13 ± 2.5
pH_{PZC}	5.7	2.6
Texture (USDA)	Sandy clay loam	Loamy coarse sand
Total metal(loid)s (mg kg^{-1})		
Fe	16,350 ± 1,061	5,650 ± 71
Ca	62,500 ± 2,828	2,426 ± 145
Al	19,930 ± 1,018	3,924 ± 749
Sb	n.d.*	n.d.

*n.d., not detected (< 0.01 µg·kg^{-1}).

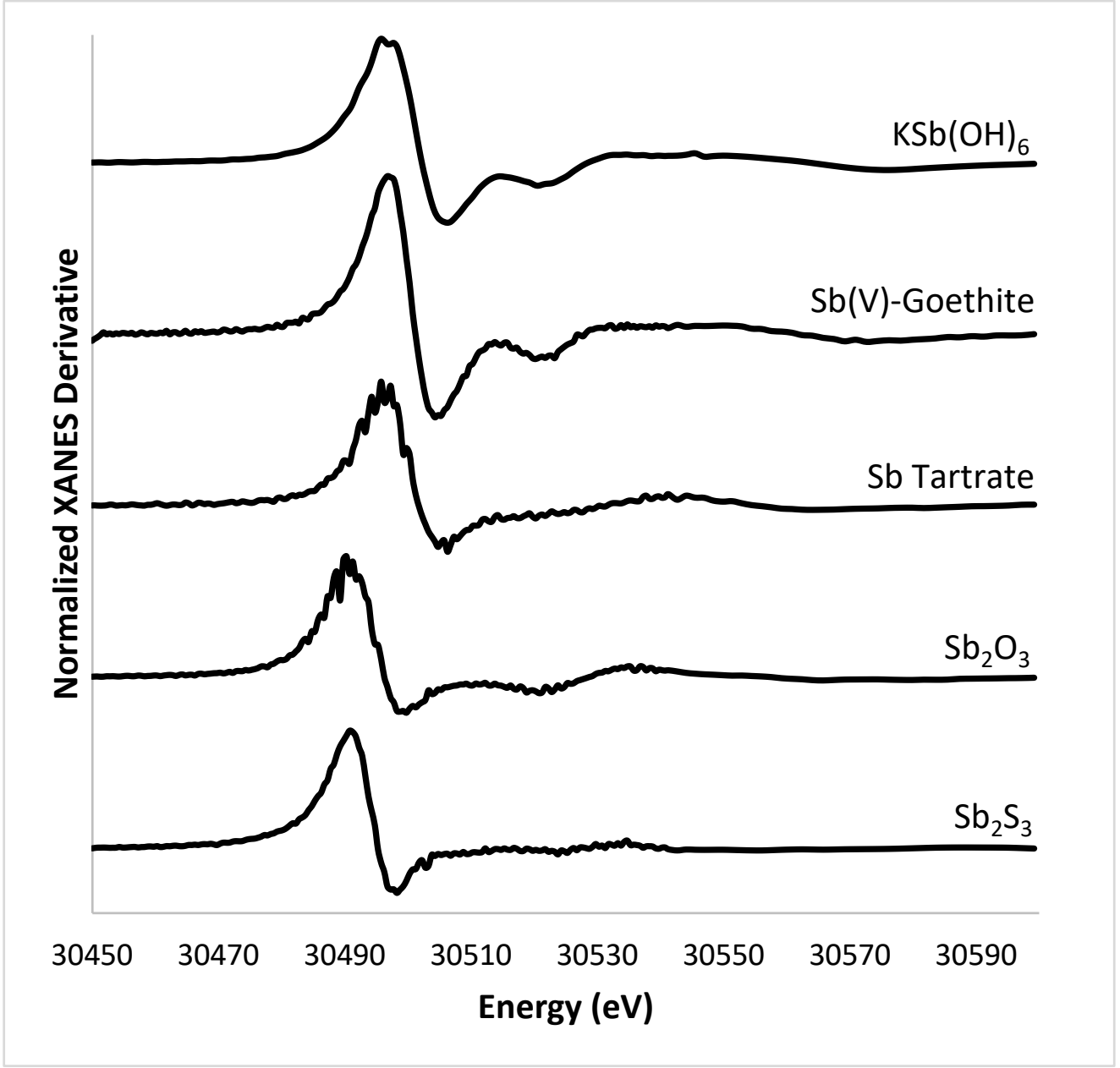

Figure S1. Derivative XANES spectra of antimony reference materials considered for linear combination fitting.

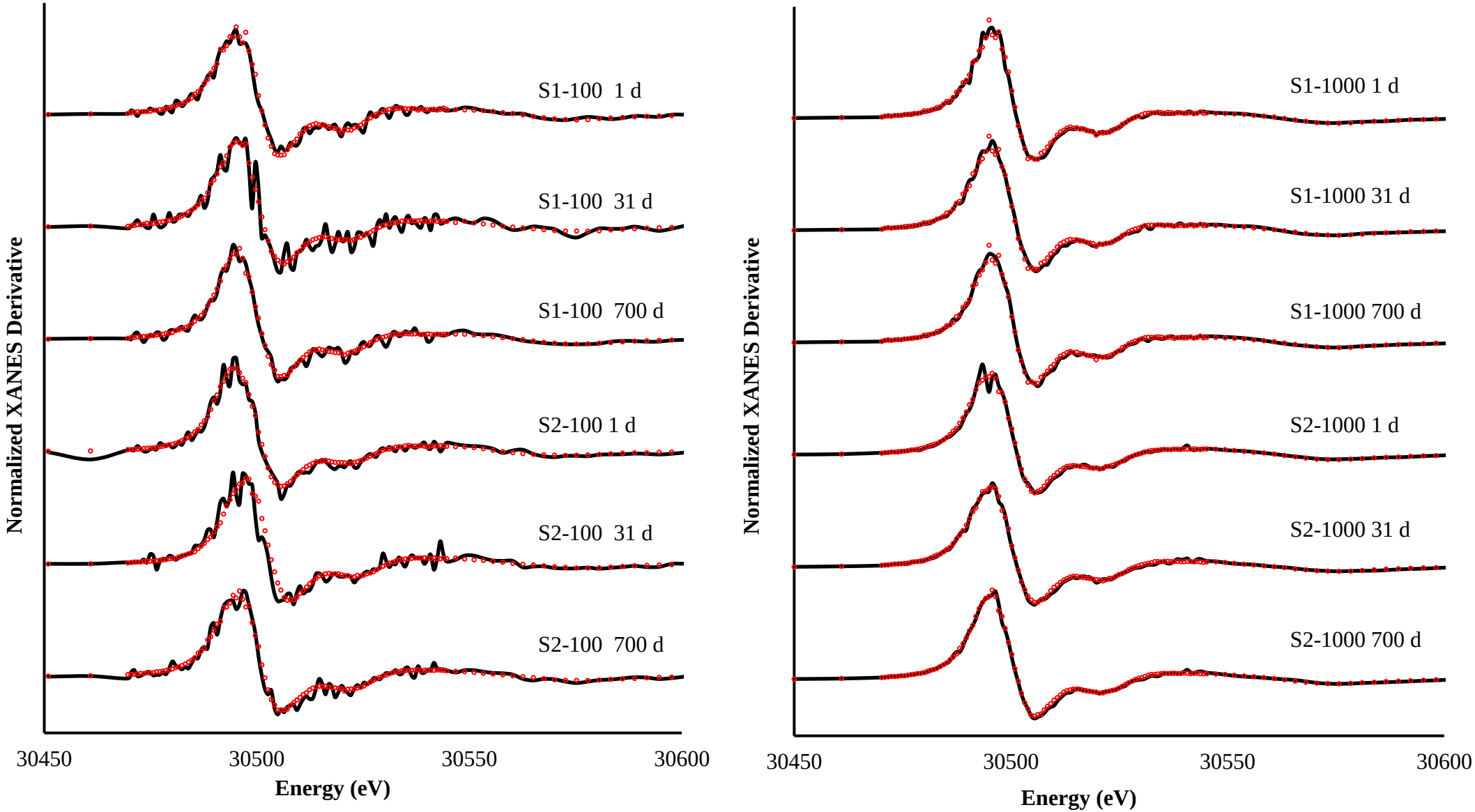

Figure S2. Derivative XANES spectra of antimony from S1 and S2 soils spiked with 100 (S-100) and 1000 (S-1000) mg Sb kg-1 soil at different ageing time. Black curves represent sample data while red curves represent LCF results. Processed results are presented in Table 4.